A Unilateral Active Knee Exoskeleton to Assist Individuals With Hemiparesis—A Pilot Study

Andrea Pergolini, Clara Beatriz Sanz-Morère, Chiara Livolsi, Matteo Fantozzi, Filippo Dell'Agnello, Tommaso Ciapetti, Alessandro Maselli, Andrea Baldoni, Emilio Trigili, *Member, IEEE*, Simona Crea, and Nicola Vitiello

***Abstract*—Most individuals who experience a stroke exhibit several sensorimotor impairments that limit their independence in everyday activities. Hemiparetic gait is frequently characterized by reduced knee flexion in swing due to knee stiffness or muscle weakness and knee hyperextension or knee buckling in the stance phase. Recently, unilateral-powered orthoses have been designed to overcome the limitations of the passive knee–ankle–foot orthoses. This study presents a unilateral active knee orthosis exoskeleton, AKO-β, endowed with a series-elastic actuator and designed to assist the knee in flexion and extension movements. In this article, we describe the system mechatronic design and its characterization on the bench, the control system, and pilot experiments with three poststroke participants. The device has a weight of 1.78 kg on the user's leg, with a lateral encumbrance of 76 mm. The pilot experiments aimed to verify the effects of the exoskeleton assistance in hemiparetic gait patterns. When walking with the device, participants on average increased the knee flexion on the paretic side by 18.70° (+44.9%) during swing and decreased knee hyperextension in stance by 4.50°, compared to walking without it. Overall, when walking with the exoskeleton, subjects showed an improved gait variable score of the paretic knee profile by 37.5% compared to walking without it. The temporal and spatial gait symmetry indices did not show clear changes, although an improvement in symmetry was observed in two of the three participants. These preliminary results suggest the potential benefits of the unilateral active knee orthosis exoskeleton to enhance and restore mobility in individuals with hemiparetic gait.**

***Index Terms*—Gait phase estimation, gait rehabilitation, knee exoskeleton, poststroke.**

Received 25 October 2024; revised 26 April 2025 and 8 July 2025; accepted 6 August 2025. Date of publication 16 September 2025; date of current version 29 September 2025. This work was supported in part by European Commission under the CYBERLEGs Plus Plus Project under Grant 731931, within the H2020 framework (H2020-ICT-25-2016-2017), and in part by the Italian Ministry of Research, under the complementary actions to the NRRP "Fit4MedRob - Fit for Medical Robotics" under Grant PNC0000007. This article was recommended for publication by Associate Editor H. Zhao and Editor K. Mombaur upon evaluation of the reviewers' comments. *(Andrea Pergolini and Clara Beatriz Sanz-Morère are co-first authors.) (Corresponding authors: Andrea Pergolini; Nicola Vitiello.)*

This work involved human subjects or animals in its research. Approval of all ethical and experimental procedures and protocols was granted by the local Ethics Committee of Area Vasta Centro Toscana, Italy, notified to the Italian Ministry of Health, under Application No. 16454_spe, and performed in line with the Declaration of Helsinki.

Andrea Pergolini, Chiara Livolsi, Filippo Dell'Agnello, Andrea Baldoni, and Emilio Trigili are with the The BioRobotics Institute, Scuola Superiore Sant'Anna, 56127 Pisa, Italy, and also with the Department of Excellence in Robotics and AI, Scuola Superiore Sant'Anna, 56127 Pisa, Italy (e-mail: andrea.pergolini@santannapisa.it; chiara.livolsi@santannapisa.it; emilio.trigili@santannapisa.it).

Clara Beatriz Sanz-Morère was with the The BioRobotics Institute, Scuola Superiore Sant'Anna, 56127 Pisa, Italy. She is now with the Center for Automation and Robotics, Spanish National Research Council, 28690 Madrid, Spain (e-mail: clara.sanzmorere@csic.es).

Matteo Fantozzi was with the The BioRobotics Institute, Scuola Superiore Sant'Anna, 56127 Pisa, Italy. He is now with the IUVO S.r.l., 56025 Pontedera, Italy (e-mail: matteo.fantozzi@iuvo.company).

Tommaso Ciapetti is with the Institute of Recovery and Care of Scientific Character (IRCCS) Fondazione Don Carlo Gnocchi, 50143 Firenze, Italy.

Alessandro Maselli was with the IRCCS Fondazione Don Carlo Gnocchi, 50143 Firenze, Italy. He is now with the Dipartimento delle Professioni Tecnico Sanitarie, della Riabilitazione e della Prevenzione Azienda USL Toscana Sudest, 52100 Arezzo, Italy.

Simona Crea and Nicola Vitiello are with the The BioRobotics Institute, Scuola Superiore Sant'Anna, 56127 Pisa, Italy, also with the Department of Excellence in Robotics and AI, Scuola Superiore Sant'Anna, 56127 Pisa, Italy, and also with the IRCSS Fondazione Don Carlo Gnocchi, 50143 Firenze, Italy (e-mail: simona.crea@santannapisa.it; nicola.vitiello@santannapisa.it).

This article has supplementary downloadable material available at https://doi.org/10.1109/TRO.2025.3610187, provided by the authors.

Digital Object Identifier 10.1109/TRO.2025.3610187

I. Introduction

STROKE prevalence has increased by 85% over the past three decades, with 12.2 million stroke events occurring worldwide in 2019 [1]. Stroke survivors often experience sensorimotor impairments, such as spasticity and hemiparesis [2], [3], leading to asymmetric, slow walking with impaired joint motion, and compensatory movements, such as hip circumduction and hip hiking [4]. In particular, the hemiparetic gait increases the risk of falling, reduces energy efficiency, and limits independence in daily activities [5]. Gait recovery is a primary goal in poststroke rehabilitation programs [6]. Still, only 50% of poststroke individuals regain independent walking after rehabilitation treatments, and the majority continue to exhibit gait deficits [7].

The characteristic kinematic patterns of individuals with hemiparetic gait often involve reduced hip flexion at the heel-strike event and during the midswing phase on the paretic side, along with insufficient dorsiflexion at the ankle joint, i.e., the foot drop [4]. Hemiparetic gait is often characterized by knee impairments that compromise both mobility and stability. During the swing phase, reduced knee flexion, caused by either muscle weakness or excessive quadriceps activity, results in a stiff knee gait [8]. In the stance phase, knee hyperextension occurs due to inadequate extensor control and might be used as a compensatory mechanism to provide weight-bearing stability. In contrast, knee buckling during stance stems from insufficient extensor strength, leading to uncontrolled knee flexion, compromising weight support [8].

To mitigate these knee impairments, mechanical stance-control knee–ankle–foot orthoses are adopted by poststroke

individuals [9], [10]. However, such orthoses may hinder weight acceptance and hamper walking on nonlevel surfaces [11]. Microprocessor-controlled orthoses offer improved stance-phase compliance by mimicking the knee's dampening function [12]. Nevertheless, they are unable to deliver positive energy.

Powered exoskeletons, instead, present the possibility of restoring the joint biomechanical function by injecting net-positive energy during the complete gait cycle. In particular, unilateral single-joint exoskeletons can benefit hemiparetic gait by selectively acting on the impaired joint and leaving the nonparetic limb free for body balance [13]. Several unilateral exoskeletons have been designed to assist the knee joint by exploiting different actuation units, ranging from pneumatic [14], [15] to variable stiffness actuators [16], [17], [18] or other conventional driving models [19], [20], [21], [22], [23]. However, several challenges remain for such devices to be commonly adopted by poststroke individuals, mostly because of their cumbersome and heavy design and limited torque controllability [24].

To achieve the closed-loop torque controllability and guarantee a compliant interaction with the user, series-elastic actuators (SEAs) are widely adopted solutions for powered knee exoskeletons [25], [26], [27], [28], [29]. SEAs can be designed to ensure higher safety, energy efficiency, shock tolerance, and back drivability compared with other types of actuators [30]. However, their compliant element might result in increased weight and encumbrance of the actuation unit compared with the conventional electrical actuation [31].

Besides the need for limited weight and encumbrance, the control scheme needs to be reliable and adaptable to the specific gait impairments of individuals [32]. Continuous gait phase estimation, particularly through adaptive oscillators (AOs) [19], [33], [34], provides a promising solution to assist specific deficits along the entire gait cycle compared with other methods [35]. For instance, the REFLEX employs AOs to track the nonassisted limb and guides the knee movement on the hemiparetic side. However, this system requires additional sensors on the unaffected leg to estimate the phase shift and deliver the assistive action [21].

This article presents a portable, unilateral active knee orthosis exoskeleton (AKO-β) based on a reaction force-sensing SEA architecture [36], implementing a control strategy based on AOs to estimate the gait phase [33]. The AKO-β SEA design incorporates a planar torsional spring that enables precise torque control with a compact design. The control system utilizes the embedded knee joint encoder to continuously estimate the gait phase from the measured hemiparetic knee joint angle, enabling phase-locked torque assistance to deal with different knee impairments. The AKO-β was tested in a pilot study involving three individuals with chronic poststroke hemiparetic gait. The objective was to explore the feasibility of using the AKO-β to mitigate knee impairments and evaluate the performance of the control system, laying the groundwork for future investigations.

II. Mechatronic Design

A. System Requirements and Overview

To design the exoskeleton, kinetic and kinematic differences between poststroke and healthy individuals were analyzed, in ground-level walking [37], [38], [39], stairs negotiation [40], [41], and sit-to-stand transitions [42]. Data are summarized in Table I. Considering an average male individual weighing between 77 and 92 kg, state-of-the-art data show that the peak torque on the paretic knee is, on average, 15–33 N·m lower than that on the nonparetic knee in sit-to-stand movements [42]. In other locomotion modes, the difference between the paretic and nonparetic peak torque is around 16–24 N·m [40]. In addition, the knee angular velocity in overground walking ranges around 100–220°/s in individuals without knee impairments walking at natural speed. Based on these considerations, the AKO-β was designed to provide a peak torque of 30 N·m during movements at relatively high speed, up to 360°/s.

In addition, the specifications for the actuator were identified in terms of weight and encumbrance. Previous biomechanical studies suggest that the total weight on the user's leg should be less than 2 kg to maintain physiological metabolic cost and walking biomechanics [43], and the lateral encumbrance should be smaller than 70 mm in the coronal plane [16] to prevent hindrance during daily activities, such as sitting or passing through doorways.

The AKO-β was designed with a single-axis joint collocated with the user's knee flexion–extension axis and with the electronic assembly located in a dedicated backpack. This simplification was done to ensure a lightweight assembly and minimize inertial effects due to the distal actuator mass on the lateral side of the limb [43].

B. Actuation Unit and Spring Design

The actuation unit of AKO-β is a single-axis reaction force-sensing SEA [36] with one rotational degree of freedom that continuously transmits the motion in the knee sagittal plane [see Fig. 1(a)]. The SEA design represents a tradeoff between compactness, weight, and the torque/speed requirements identified for the target application. Previous SEA-based architectures were developed for bilateral hip exoskeletons [44], with different performance requirements.

The actuation unit embeds a 70 W dc brushless motor (EC-45, 24 V, Maxon Motor, Sachseln, Switzerland) coupled with a Harmonic Drive (HD) reducer (CSD-17-100-2A, reduction ratio 100:1). As a reaction force-sensing SEA, the elastic element is placed between the actuator ground and the shared frame of the motor and the HD, as shown in Fig. 1(b).

The elastic element of the SEA is a torsional spring (patent no. WO2020104962A1 [45]), shaped as a hollow planar design and thickness of 4 mm to reduce the lateral encumbrance in the actuator assembly. The grooves on the spring were obtained through wire electrical discharge machining, dimensioned using finite-element simulation, and sized to achieve a stiffness comparable with the quasi-stiffness of the knee joint of healthy users of 75 kg in the weight acceptance phase of walking (240 N·m/rad) [46]. Experimental characterization demonstrates angle–torque linearity ($R^2 = 0.99$) with the linear fit reported in Fig. 1(c) and negligible hysteresis. In detail, the inner ring of the spring is coupled with the actuation frame, while the outer ring is connected to the actuator ground. This, in turn, is coupled to the user's thigh via the physical human–robot interface. The

TABLE I
KNEE BIOMECHANICAL FEATURES OF POSTSTROKE AND HEALTHY INDIVIDUALS DURING VARIOUS ACTIVITIES

	Walking		Stair negotiation		Sit-to-Stand/Stand-to-Sit	
	Healthy individuals	**Individuals following a stroke**	**Healthy individuals**	**Individuals following a stroke**	**Healthy individuals**	**Individuals following a stroke**
Range of movement	Min: 5° Max: 65°	Min: -5° Max: 40°	Min: 0° Max: 112°	Min: 0° Max: 101°	Min: 0° Max: 100°	Min: 0° Max: 100°
Peak angular velocity	Flexion: 209°/s Extension: −220°/s	Flexion: 190°/s Extension: −202°/s	Ascent: 102°/s Descent: 129°/s	Ascent: 100°/s Descent: 135°/s	Stand-to-sit: 142°/s Sit-to-stand: 181°/s	Stand-to-sit: 142°/s Sit-to-stand: 181°/s
Peak torque	Flexion: 35 N·m Extension: −18 N·m	Flexion: 16 N·m Extension: − 23 N·m	Ascent: −82 N·m Descent: −86 N·m	Ascent: −58 N·m Descent: −70 N·m	Stand-to-sit: 72 N·m Sit-to-stand: 88 N·m	Stand-to-sit: 57 N·m Sit-to-stand: 55 N·m

Angular velocity and torque are negative in extension and positive in flexion.

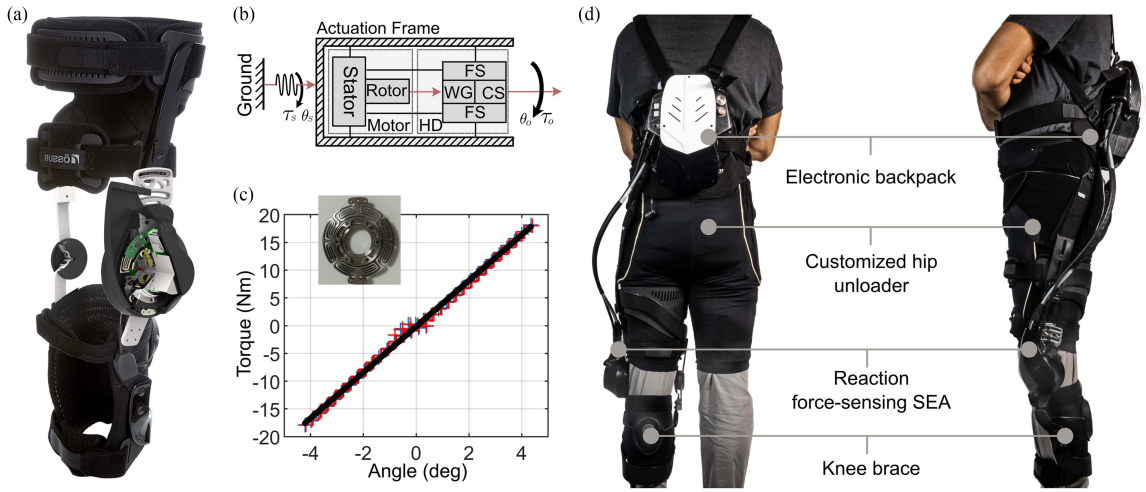

Fig. 1. Compliant active knee exoskeleton (AKO-β). (a) Sectional view of the actuation unit and the customized contralateral passive joint embedded in the commercial knee brace (Össur Rebound PCL). (b) Reaction force-sensing SEA architecture of the AKO-β. (c) Custom planar torsional spring, experimental characterization, and linear fit. (d) Posterior and lateral views of the AKO-β donned by a healthy person.

motor is coupled to the HD by linking the motor rotor to the wave generator and the flexspline to the motor stator. The final stage of the transmission is the HD circular spline connected to the output link, which is tightened to the shank of the user.

The knee angle (θ_p) is measured by a 13-bit absolute magnetic encoder (RMB20, RLS Merilna tehnika d.o.o., Komenda, Slovenia) and the torque (τ_s) is calculated using the spring deformation, measured by a dedicated 20-bit magnetic absolute encoder (AksIM-2 MB080 readhead with MRA080 ring, RLS Merilna tehnika d.o.o., Komenda, Slovenia) fixed to the ground, achieving a torque resolution of 1.44 N·mm.

The resulting reaction force-sensing SEA unit has a weight of 0.884 kg, a lateral encumbrance of 76 mm, and a sagittal length of 114 mm.

C. Physical Human–Robot Interface

The physical human–robot interface is a customized version of a commercial knee brace (Rebound PCL, Össur, Reykjavik, Iceland). In particular, the embedded passive joints were removed and substituted with the SEA on the external side and with a single ball bearing on the internal side. The weight of the brace is supported by a vertical Velcro latch attached to customized trousers (Unloader Hip, Össur, Reykjavik, Iceland) that the user wears before donning the exoskeleton. The actuation unit is embedded within the brace, exploiting the lateral concave space above the contralateral ligament of the knee joint to reduce encumbrance, as shown in Fig. 1(d). Finally, to accommodate the range of motion (ROM) of the human knee, the AKO-β was designed to cover a ROM of 130°, with 0° with the knee fully extended. In addition, a mechanical stop limits the exoskeleton's range of movement at 0° to avoid mechanical stress against the user's rotula and guarantee a safe use.

The mass of AKO-β on the leg of the user is 1.780 kg, including the weight of the actuation unit and the customized physical human–robot interface.

D. Electronic Backpack and Embedded Power Electronics

The power and control electronics and the battery were enclosed in a dedicated backpack, connected to the actuation unit via a custom-made shielded cable with fast-lock connectors (MINIMAX-24 and ULTIMATE-3 Fischer Connectors, Saint-Prex, Switzerland). The electronic backpack was designed to be easy to wear, lightweight, and ergonomically shaped to fit the

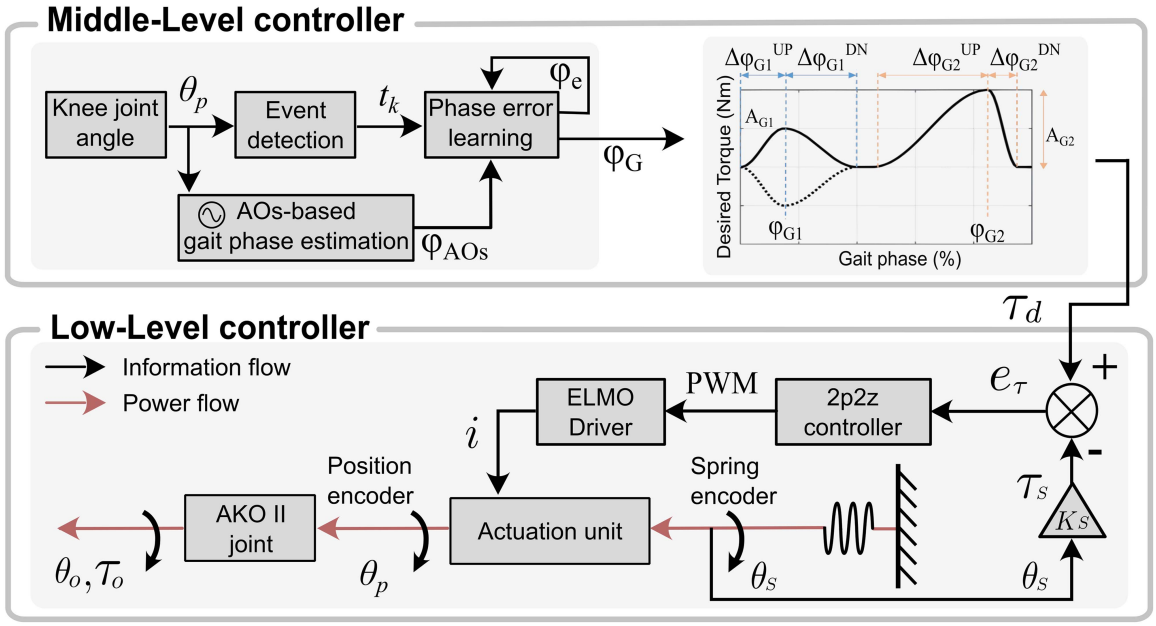

Fig. 2. AKO-β control system based on a two-layer hierarchical architecture. The middle-level controller is composed of the event detector, the AOs-based gait phase estimator, the phase error learning, and the phase-locked torque designer. The low-level layer implements a closed-loop torque control through a two poles–two zeros compensator.

lumbar concavity [see Fig. 1(d)]. The technology core is composed of two stacked custom printed circuit boards (PCBs). The first one embeds a system-on-module (SbRIO-9651, National Instruments, Austin, Texas, USA) with an field-programmable gate array (FPGA) (Zynq7020, Artix7) and an ARM processor (Zynq7020, 667 MHz, ARM Cortex-A9) endowed with a real-time operating system that runs the control system. In addition, the AKO-β embeds a commercial nano router WiFi (TP-Link WR802N) used to connect the exoskeleton to an auxiliary remote PC and a microSD card for data storage.

The second custom PCB embeds the following:

1) electrical safety circuits;
2) a dc/dc converter to translate reliably the voltage levels and proper power delivery;
3) a digital driver ELMO Gold Twitter 15/100 to manage the three-phase brushless motor;
4) an electromagnetic interference filter to comply with the directive of biomedical devices class II-A (EN 60601-1).

In addition, the motor driver implements the safe torque off standard to disable the motor movement via hardware when an emergency button (BINDER three-way connector) is connected and pressed.

The AKO-β is powered by an eight cells lithium-ion battery (Panasonic cells, 2900 mA/h, 83.52 Wh) equipped with a battery management system and plugged inside the backpack. The total weight of the electronic backpack and battery (0.630 kg) on the user's back is 2.370 kg.

E. Control

The AKO-β control system is based on a two-layer hierarchical architecture (see Fig. 2): First, the middle level estimates the gait phase in real time and computes the desired assistive torque, and second, the low-level layer is responsible for the closed-loop torque control. In this work, the user's locomotion mode (ground-level walking) is manually selected by the user.

1) Middle-Level Controller: The AKO-β middle-level controller sets the desired torque as a function of the gait cycle in rhythmic tasks (e.g., walking and stair negotiation) [33]. In these tasks, the middle-level controller is based on the following:

1) a pool of AOs that estimates in real time a continuous gait phase variable φ_{AOs};
2) an event detection algorithm;
3) a phase error learning that computes the phase error (P_e) at the instant of the detected event and compensates it by smoothly correcting φ_{AOs};
4) a phase-locked torque designer for the definition of the desired torque (τ_d).

A detailed description of the phase estimator architecture is given in [33]. The main features are recapped hereafter for the sake of clarity.

The *AOs-based gait phase estimator* decomposes the input signal, the knee joint angle, into its different harmonics. In particular, the pool of AOs captures the fundamental features of a quasi-periodic input signal, i.e., the phase (φ_{AOs}), frequency (ω), amplitude, and offset of each harmonic. The input signal is then reconstructed in real time, exploiting the learned features. The difference between the input signal and the reconstructed input drives the evolution of the dynamic system.

The *gait event detector* identifies the beginning of each gait cycle during quasi-periodic activities, such as walking or negotiating stairs. The most common event used to detect a new gait cycle is the heel strike, which is not easily estimated from the knee angle signal. Consequently, the maximum knee flexion

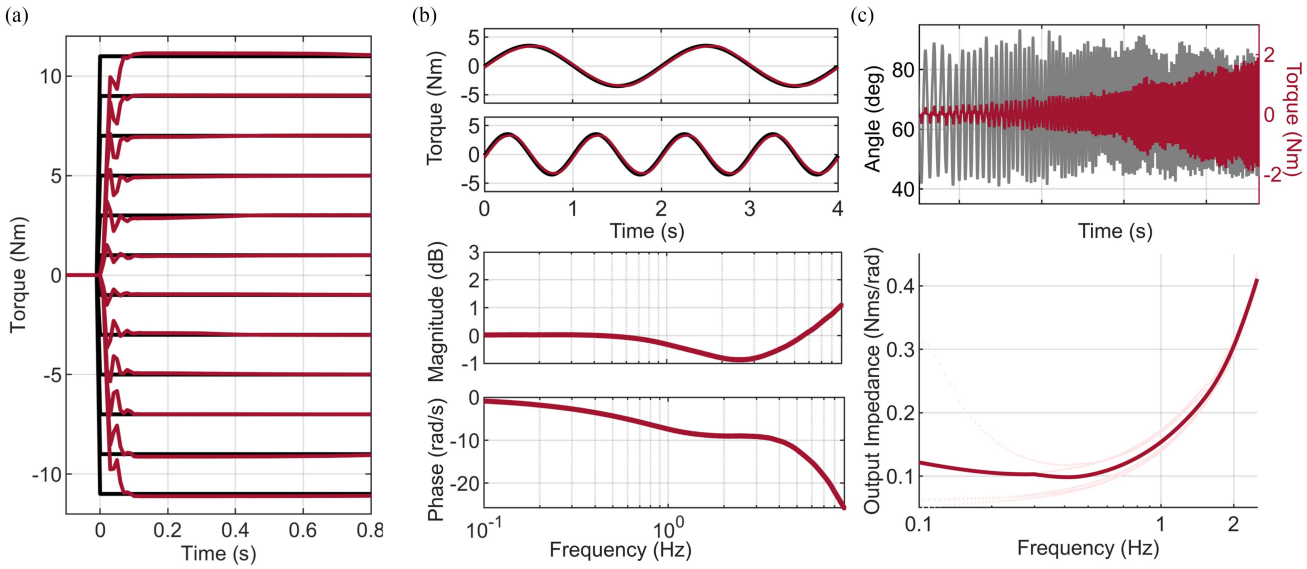

Fig. 3. Experimental results of the characterization of the closed-loop torque control. (a) Step response tests. (b) Chirp response (top panels) and bode plot of the closed-loop system (bottom panels). (c) Measured angle and torque (top panel) and bode plot (bottom panels) for the output impedance test.

was selected for the real-time segmentation of the gait cycle, similar to the control strategy previously implemented for a hip exoskeleton [33].

Ideally, the gait phase of a locomotion cycle should be a linear monotonic signal that increases from 0 to 2π (φ_{LIN}), where 0 is the beginning of the new cycle (here, the maximum of the knee angle happens during the swing for the walking task). Once the gait event is detected, *a phase error learning block* calculates the phase reset error as follows:

$$P_e\ (t_k) = \begin{cases} -\ \varphi_{\text{AOs}}\ (t_k)\ , \text{ if } 0 \leq \varphi_{\text{AOs}}\ (t_k) \leq\ \pi \\ 2\pi -\ \varphi_{\text{AOs}}\ (t_k)\ , \text{ if } \pi \leq \varphi_{\text{AOs}}\ (t_k) \leq 2\pi. \end{cases}$$

To avoid abrupt compensation of the calculated phase reset error, a state variable (φ_e) learns $P_e(t_k)$ and smoothly compensates for this error within the current gait cycle by subtracting φ_e from φ_{AOs} to obtain the smoothed gait phase φ_G.

The desired torque profile is a function of the estimated gait phase. In particular, τ_d is defined using asymmetric Gaussian curves that can be tuned in amplitude (A_{GX}), peak phase (φ_{GX}), and rising and falling duration ($\Delta{\varphi_{GX}}^{\text{UP}}$, $\Delta{\varphi_{GX}}^{\text{DN}}$); an offset ($\alpha_0$) can be added. Fig. 2 presents an example of a possible desired torque profile with two Gaussian functions.

2) Low-Level Controller—Bench-Test Characterization: The low-level control implements a closed-loop regulator that sets the reference current to the motor driver i based on the error (e_d) between τ_d and the measured torque (τ_s) (see Fig. 2). The closed-loop torque control consists of a two poles–two zeros compensator, the performance of which was assessed by analyzing:

1) the response to torque steps;
2) the response to torque chirps;
3) the system output impedance when τ_d is set to 0.

To assess the responses to torque steps and chirps, the output link of the actuator was mechanically locked on a test bench. For the step response analysis, positive and negative torque steps were commanded from -11 to 11 N·m. Each step amplitude was repeated five times. The mean and standard deviation (std) of the measured torque for each torque step amplitude are shown in Fig. 3(a). Table II reports the mean ($\pm$ std) values between step repetitions of the rise time, settling time, and overshoot percentage for all steps.

For the chirp response, a chirp signal of 4 N·m torque amplitude ranging from 0.1 to 9 Hz in 280 s was commanded to the low-level controller. The test was repeated five times. The resulting bode diagram is reported in Fig. 3(b), and the estimated -3 dB bandwidth was above 9 Hz.

Finally, to evaluate the output mechanical impedance of the exoskeleton, the output link was driven manually by an experimenter following a sinusoidal chirp motion of 20° of amplitude and frequency ranging from 0.1 to 2.5 Hz in 120 s, while τ_d was set to 0. Each test was repeated five times and the transfer function between τ_s and $\dot{\theta}_p$ was calculated. The upper part of Fig. 3(c) reports a maximum parasitic torque over the analyzed bandwidth lower than 1.75 N·m. Moreover, considering frequencies up to 1 Hz, the maximum parasitic torques resulted in lower than 0.75 N·m. The mean bode diagram over all the repetitions is shown in the lower part of Fig. 3(c) and ranged from 0.1 N·ms/rad up to 0.4 N·ms/rad over the explored frequency range.

III. Pilot Experiments With Poststroke Participants and Results

A. Study Participants and Experimental Protocol

A pilot experiment with individuals following a stroke was conducted to verify preliminary that whether the assistive action provided by the knee exoskeleton could mitigate knee impairments and lead to more physiological gait patterns.

Three participants with mild-to-moderate gait impairments due to a stroke were recruited for this study. The inclusion criteria included the following:

TABLE II
MEAN (± STANDARD DEVIATION) OF THE STEP RESPONSE CHARACTERIZATION

Steps (N·m)		Steady-state Error (N·m)		Rise time (ms)		Settling time (ms)		Overshoot (%)	
+1	−1	−0.06(±0.08)	−0.08(±0.03)	21.7 (±0.8)	21.5 (±0.2)	52.8 (±6.0)	62.0 (±2.1)	8.43 (±2.0)	11.0 (±0.6)
+3	−3	0.03(±0.02)	0.01(±0.02)	20.8 (±0.2)	20.7 (±0.1)	53.2 (±1.4)	60.4 (±1.3)	10.5 (±0.6)	14.0 (±0.4)
+5	−5	−0.05(±0.01)	−0.03(±0.02)	20.6 (±0.1)	20.8 (±0.1)	56.4 (±0.2)	59.1 (±0.8)	11.5 (±0.1)	13.8 (±0.5)
+7	−7	0.02(±0.01)	−0.03(±0.03)	19.9 (±0.1)	20.3 (±0.1)	59.0 (±0.2)	63.9 (±0.2)	13.1 (±0.1)	14.0 (±0.3)
+9	−9	0.02(±0.01)	−0.04(±0.06)	19.1 (±0.1)	19.8 (±0.1)	62.0 (±0.3)	69.6 (±0.2)	13.9 (±0.2)	14.3 (±0.2)
+11	−11	0.05(±0.03)	0.07(±0.01)	18.9 (±0.1)	20.2 (±0.1)	68.0 (±0.3)	77.9 (±0.6)	13.8 (±0.2)	15.1 (±0.2)

TABLE III
PARTICIPANTS' CHARACTERISTICS

ID	Age	Sex	Height	Weight	Aids	Cause of Stroke	Chronicity	Knee impairments	Treadmill speed
ID1	57	M	170 cm	76 kg	none	Hemorrhagic	36 months	Hyperextension, deficit in knee flexion during swing, stiff knee	2.7 km/h
ID2	76	M	170 cm	80 kg	none	Ischemic	48 months	Knee buckling, deficit in knee flexion during swing, knee flexor weakness	1.5 km/h
ID3	69	M	177 cm	85 kg	cane	Hemorrhagic	19 months	Hyperextension, deficit in knee flexion during swing, stiff knee	1 km/h

1) age $>$ 18 years;
2) time from the event $>$ 3 months;
3) ability of independent gait, even with assistive tools (i.e., functional ambulation classification $\geq$ 4);
4) Medical Research Council muscle strength score in the range [2, 4];
5) modified Ashworth scale score $<$ 3;
6) capability to walk on a treadmill;
7) exhibiting gait impairments on the left side since the AKO-β was designed for the left leg.

Participants were allowed to use their ankle foot orthosis, if prescribed. The exclusion criteria included the following:

1) cognitive impairment (minimental state examination score $<$ 21);
2) severe anxiety or depression (state-trait anxiety inventory $>$ 44 and beck depression inventory $>$19);
3) severe comorbidities (e.g., chronic heart failure, uncontrolled diabetes or hypertension, chronic obstructive pulmonary disease, severe hip/knee osteoarthritis, severe osteoporosis, and severe sensory deficit);
4) skin wounds or infection at interaction points with the exoskeleton interface;
5) implantable cardiac devices, such as pacemakers or automatic defibrillators;
6) physician disapproval.

The characteristics of the participants are reported in Table III. The participants were informed about the purpose of the study, the procedures, the data treatment, and all signed informed consent before starting the study. Experiments were carried out at the clinical center IRCCS Fondazione Don Carlo Gnocchi of Florence (Italy). The experimental protocol was approved by the local Ethics Committee of Area Vasta Centro Toscana, Italy (Protocol ID: CLs++2ndCS; approval number: 16454_spe), notified to the Italian Ministry of Health, and conducted in accordance with the Declaration of Helsinki.

Fig. 4 describes the experimental protocol and shows the experimental setup. For each participant, the protocol included three sessions conducted on three different days (within five days):

1) a *Tuning session,* with the goal to tune the AKO-β assistive profiles;
2) a *Familiarization session,* aimed to let the participant familiarize themselves with the exoskeleton in walking;
3) an *Assessment session,* to evaluate the impact of the AKO-β on the participant's gait kinematics.

An optical motion capture system (Smart-DX BTS Bioengineering, Milano, Italy) was used to measure and assess lower limb joint kinematics in three walking conditions: without the AKO-β (NoExo), with the exoskeleton in assistive mode (AM), and with the exoskeleton providing null torque (i.e., τ_d set to zero), namely in transparent mode (TM). Kinematic data were recorded following the dynamic and active-pixel vision sensor (DAVIS) protocol [47], attaching the markers to the structure of AKO-β when anatomical landmarks were hidden by the exoskeleton (i.e., lateral epicondyle and head of fibula on the paretic side), similarly to [48]. Participants utilizing aids for daily activities were allowed to use the treadmill handrails; consistent walking conditions were maintained across all sessions.

In the *Tuning session*, participants were requested to walk on a treadmill and clinicians helped them to identify their comfortable speed. Concurrently, clinicians observed the participants to analyze their main knee impairments. Table III reports the gait impairments and comfortable gait speed of the participants. Subsequently, participants donned the AKO-β with the help of an experimenter and walked on the treadmill for up to 20 min in 3- to 5-min bouts. Between each walking bout, participants rested for at least 5 min. During these trials, an experimenter tuned the assistive torque profiles. The assistive profile was set with a peak torque of at least 0.1 N·m/kg, and parameters were

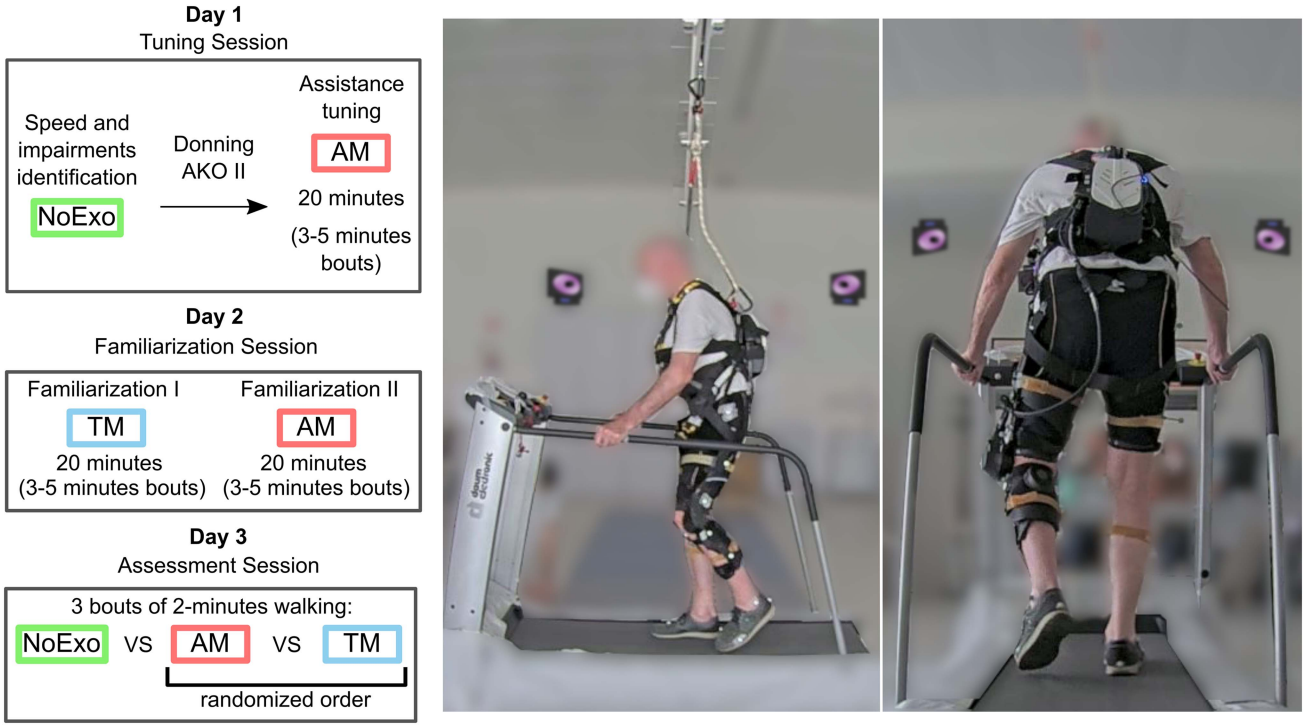

Fig. 4. Experimental protocol and setup. The tuning session included three objectives: the identification of the knee impairments, the identification of the self-selected comfortable speed on the treadmill without the AKO-β (NoExo), and the definition of the assistive parameters. The familiarization session included walking trials for at least 20 min with the AKO-β in AM and in TM. The assessment session included three 2-min walking bouts, one for each condition.

adjusted to ensure the user's comfort and safety and mitigate the specific knee impairments.

During the *Familiarization Session*, participants donned the AKO-β and were prepared for a gait analysis acquisition. During this session, they walked on the treadmill for at least 20 min with the assistive parameters tuned during the previous session (AM), and at least 20 min in TM. The walking time was divided into several 3- to 5-min bouts, depending on the subject's perceived fatigue. The 20 min were selected to match the amount of time reported for healthy participants as the minimum time necessary to adapt to an assistive device [49]. A dedicated session for familiarization was considered to avoid fatigue bias in the subsequent assessment session.

In the *Assessment Session*, participants were asked to perform three bouts of 2-min walking on the treadmill: one bout without wearing the exoskeleton (NoExo), one while wearing the exoskeleton controlled in AM, and one while wearing the exoskeleton in TM. Kinematic data from the motion capture were collected during the last minute of each 2-min walking bout. The NoExo condition was always carried out at the beginning to capture natural walking of participants and avoid the risk of observing alterations in gait kinematics due to the use of the exoskeleton. Then, the AM and TM conditions were carried out in a randomized order. The three conditions (NoExo, AM, and TM) were not randomized fully, also to avoid donning and doffing the AKO-β several times, and thus to avoid a short but necessary additional time to ensure the proper fit of the exoskeleton. Prior to the two bouts with the AKO-β, participants were asked to walk for 5 min on the treadmill for additional familiarization. Participants rested for at least 5 min between each walking task to avoid fatigue.

B. Data Analysis

Data were recorded by the onboard sensors of the AKO-β, with a sampling frequency of 100 Hz, and by the motion capture system at 250 Hz. Data collected by the motion capture system were initially analyzed offline by an integrated stand-alone software package (Smart Analyzer, BTS, Milan, Italy) used to obtain the 3-D coordinates of the markers and the lower limb kinematic patterns.

Signals from the AKO-β and the motion capture system were temporally aligned using an external synchronization signal sent and recorded at the beginning and end of each task to both devices. All data were then segmented into single strides based on the heel strike detected from the 3-D coordinates of the markers, following the methods described in [50]. Medians and percentiles (25th, 75th) of the lower limb kinematics profiles normalized by the stride duration were calculated for each participant.

Three biomechanical features were computed on the paretic side to quantify possible effects of the exoskeleton assistance:

1) the maximum knee flexion angle during the swing phase;
2) the maximum knee extension angle during the stance phase;
3) the gait variable score (GVS) [51], computed as the root-mean-square (RMS) difference of the paretic knee angular profile and the physiological angular profile [37].

IEEE Transactions on Robotics (T-RO) paper, presented at ICRA 2026, Vienna, Austria. Cite as T-RO paper.

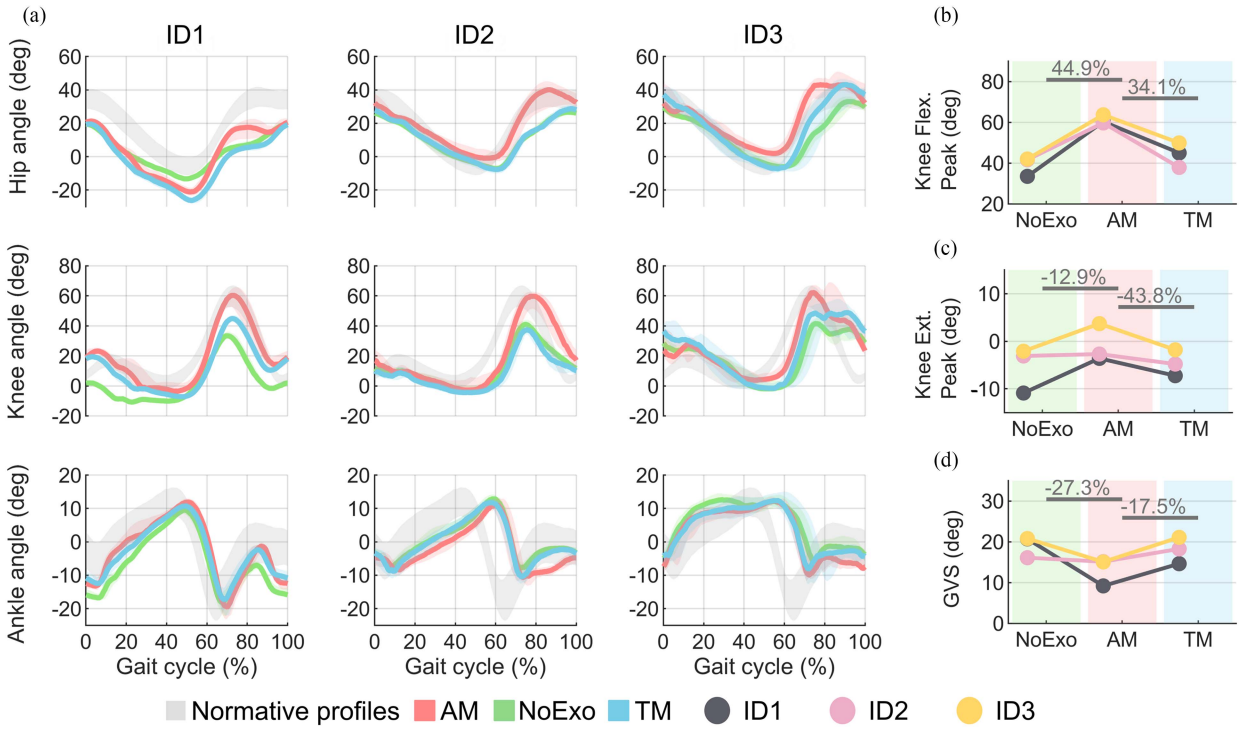

Fig. 5. Participants' gait kinematics. (a) Hip, knee, and ankle angular profiles of the paretic side of the three participants in three walking conditions (NoExo, TM, and AM). Profiles are shown as medians and 25th, 75th percentiles. (b) Knee angle peak in flexion, peak in extension, and GVS.

In addition, the ROMs of the hip, knee, and ankle were computed. These performance indicators were computed in all the segmented strides and then described for each subject as median and percentiles (25th, 75th).

Data from the motion capture system were also used to compute temporal and spatial symmetry ratios (SRs) between nonparetic and paretic sides, respectively, using the swing duration (% gait cycle) and the step length (cm) [52]. Perfect symmetry is given by an SR of 1. Temporal and spatial SRs were computed in all the segmented strides and then described for each subject as median and percentiles (25th, 75th).

Between-participants statistical analysis was not performed due to the limited sample size. However, percentage variations between the median values of the three walking conditions (AM, TM, and NoExo) were calculated to identify trends between participants.

Signals collected from the onboard sensors of the AKO-β were used to quantify the performance of the gait phase estimator. Signals were segmented into strides based on the gait phase estimated online. The performance of the AKO-β gait phase estimator was evaluated using three key indicators from [33] and [34]:

1) the RMS of the phase error;
2) the RMS of the phase reset error;
3) the linearity of the estimated phase.

The *RMS of the phase error* was computed as the error between the estimated gait phase φ_G and a linear gait phase (φ_{LIN}) spanning linearly from 0 to 2π rad within each stride.

RMS of the phase reset error is computed as follows:

$$\text{RMS}_{P_e} = \sqrt{\sum_{i=1}^{N} \frac{P_e(i)^2}{N}}$$

where $P_e(i)$ is the phase reset error P_e of the ith stride and N is the number of strides.

Linearity of the estimated phase φ_G, namely the standard deviation of the first derivative of φ_G for each stride.

The indicators were calculated offline separately for each participant and condition. Median values and percentiles (25th, 75th) were calculated across participants, separately for each condition.

C. Results

1) Gait Kinematics of Poststroke Participants: The hip, knee, and ankle angle profiles of the three participants in the three walking conditions (NoExo, AM, and TM) are reported in Fig. 5(a) along with normative profiles [37].

Walking with AKO-β in AM led to increased knee flexion during the swing phase by 18.70° and 15.36°, compared to walking without the device (NoExo) or with the device in TM, respectively [see Fig. 5(b)]. Hence, the ROM of the paretic knee increased by 41.7% (18.51°) compared with the NoExo condition, surpassing the minimal clinically important difference (MCID) that is 8.48° [53]. Increased ROM due to the exoskeleton assistance was also observed on the paretic hip (an increase of 16% in the comparison between AM and NoExo).

TABLE IV
COMPARISON OF SEAS AND THE SPECIFICATIONS OF KNEE EXOSKELETONS FOR POSTSTROKE INDIVIDUALS

Knee Exo	Actuator weight	Weight on the leg	Encumbrance	Peak/constant torque	Spring/Stiffness
AKO-β	**0.88 kg**	**1.78 kg**	**Lateral: 76 mm Sagittal: 114 mm**	**30 N·m/ 25 N·m**	**planar torsional spring 240 N·m/rad**
SERKA [22]	-	1.20 kg (without actuation unit)	Lateral: - Sagittal: 100 mm	45 N·m / 40 N·m	Torsional spring 24 N·m/rad
Utah Knee [25]	0.79 kg	3.60 kg	Frontal: 70 mm Sagittal: -	120 N·m/	Linear spring
M. Shepherd [26]	1.80 kg	4.10 kg	Lateral/Sagittal: -	80 N·m/ 40 N·m	cantilever fiberglass beam 274 N/mm
Active Knee Orthosis [27]	1.70 kg	3.80 kg	Lateral: 90 mm Sagittal: -	70 N·m/ 50 N·m	Torsional spring 150 N·m/rad
cRSEA [28]	-	-	Lateral/Sagittal: -	130 N·m/ 10 N·m	torsional spring between gears 0.30 N·m/rad
AssistOn-Knee [29]	-	1.4 kg (without actuation unit)	Lateral/Sagittal: -	780 N·m / 35 N·m	Linear spring

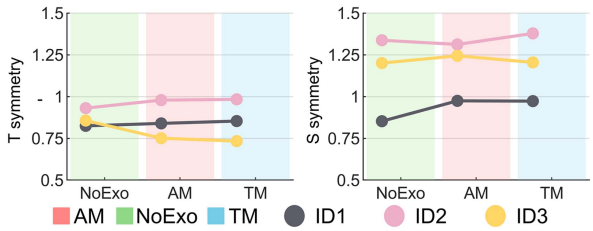

Fig. 6. Median values of each participant of the temporal and spatial gait SR.

The assistance provided by the AKO-β led to reduced knee extension angle during stance, with reductions by $-4.50°$ compared with the NoExo condition, and by $-3.75°$ compared with the TM condition [see Fig. 5(c)].

The AKO-β assistance improved the GVS of the paretic knee by 27.3% compared with the NoExo condition and by 17.5% compared with the TM condition [see Fig. 5(d)].

Detailed results are reported in the Supplementary Material Table S1.

Concerning symmetry, different results were observed when considering temporal and spatial SRs. The assistance of the AKO-β led to improved spatial symmetry for ID1 (from 0.85 in NoExo to 0.97 in AM) but had no evident effects on the temporal SR; for ID2, the assistance led to improved temporal SR (from 0.93 in NoExo to 0.98 in AM), without evident improvements for the spatial SR.

Detailed data for each participant in the three walking conditions are reported in Fig. 6 and in the Supplementary Material Table S1.

2) Performance of the Gait Phase Estimator: Concerning the performance of the phase estimation algorithm, the knee angle, torque, and power computed by exoskeleton are shown in Fig. 7(a), and the estimated gait phase φ_G in AM is shown in Fig. 7(b).

The RMS phase error against φ_{LIN} was 0.39% of the gait cycle in AM and 0.56% of the gait cycle in TM.

The RMS$_{Pe}$ resulted equal to 1.71% of the gait cycle in AM and 2.87% of the gait cycle in TM.

The linearity of the estimated phase resulted equal to 0.38% gait cycle/s in AM and 0.56% gait cycle/s in TM.

Detailed results for each participant and condition are reported as a boxplot in Fig. 7(c).

IV. DISCUSSION

A. AKO-β Mechatronic Design and Performance

The total weight of AKO-β on the user's leg is 1.78 kg, with 0.88 kg attributed to the actuation unit, and a lateral encumbrance of 76 mm. These features make the design advantageous compared with other state-of-the-art SEA-based knee exoskeletons for poststroke, as summarized in Table IV [22], [25], [26], [27], [28], [29], despite the lateral encumbrance exceeding the original specification by 6 mm. Although the design process did not include direct input from potential end users from the beginning, a comprehensive review of existing devices was performed to ensure the inclusion of key functional requirements. Specifically, weight, encumbrance, and torque–speed characteristics were defined based on the biomechanical considerations and the specifications of comparable devices in the state-of-the-art, some of which incorporated clinical and end-user feedback.

In detail, the series-elastic remote knee actuator (SERKA) developed for poststroke individuals exhibiting stiff knees achieved a weight of 1.20 kg on the user's leg. However, such weight does not include the actuation unit, which is remotely located [25]. The Utah ExoKnee has a weight of 3.60 kg on the user's leg [26]. Its design exploits the top of the thigh segment to locate the actuation unit and electronics with almost no lateral encumbrance. In addition, the device can fit the left or right

IEEE Transactions on Robotics (T-RO) paper, presented at ICRA 2026, Vienna, Austria. Cite as T-RO paper.

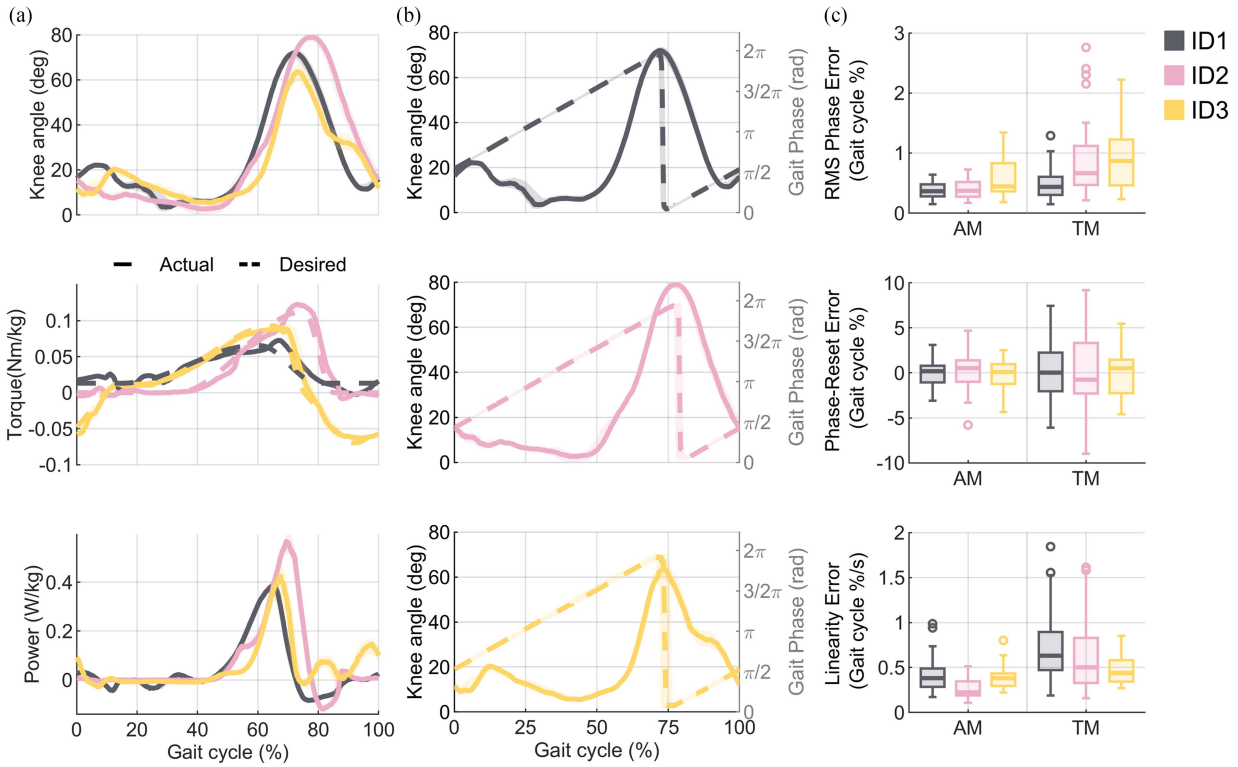

Fig. 7. Performance of the middle-level controller of the AKO-β in AM. Profiles are shown as median (25th, 75th percentile). (a) Knee angle, measured and desired torque, and power profiles on the gait cycle (0% corresponds to the heel strike). (b) Knee angle profile and gait phase estimated in real time by the middle-level controller. The 0% of the online estimated gait phase is at the knee flexion angle peak. (c) Box plots of the RMS phase error, phase reset error, and linearity error.

leg according to the user's needs. The frontal encumbrance presents advantages and disadvantages, such as, respectively, the possibility to distribute the weight on the thigh comfortably and the hindrance of the natural arm motion during sit-to-stand activities, which makes the task not natural for individuals with movement impairments. The knee exoskeleton designed by Shepherd and Rouse [27] has an actuation unit with a weight of 1.80 kg; the design exploits a cantilever fiberglass beam as the elastic element of the SEA. Finally, the actuation unit of a previous version of the knee exoskeleton designed within our laboratory weighs 1.70 kg, almost twice as much as the current version; key design features were the possibility to fit the actuation unit on the left or right leg, depending on the user's needs, and a variable transmission ratio to accommodate various locomotion modes [22].

Variable stiffness actuators present the advantage of dynamically changing the physical stiffness of the actuator compared with SEAs, allowing for better adaptation to different tasks and increasing the energy storage capacity and actuator bandwidth [16], [17], [18], but with a more complex structure and bulkier driving system [24]. The actuator with adjustable-rigidity and embedded sensor (ARES), designed to be used in an exoskeleton for children, stands out for its weight (0.90 kg), which is similar to the presented prototype, and for the minimal lateral encumbrance (around 50 mm) [16]. However, it uses a ball screw mechanism to change the actuation stiffness, which results in a bulky structure (253 mm of sagittal encumbrance) while also causing a lack of controllability in stiffness variation [20].

The dual reduction actuator of the gait enhancing mechatronics system (GEMS) L-Type exoskeleton designed for elderly individuals achieved a weight of 0.43 kg; however, this weight does not include the knee joint mechanism made of two six rolling cams, which brings the assistance to the knee joint [54]. The lightweight design of the GEMS L-Type may result in reduced performance in terms of torque control [54].

Notably, the AKO-β maximum assistive torque of 30 N·m was lower compared with state-of-the-art SEA actuators [16], [25], [26], [27], [28], [29] and in line with the GEMS system [54].

To prioritize portability, the AKO-β was built around a commercially available brace and designed without self-alignment mechanisms, a feature included in other state-of-the-art technologies, such as the Utah Exo Knee [26] and the GEMS [54]. While this design decision is advantageous to limit the device weight and encumbrance and may facilitate the transition to a commercial device, it introduces limitations in mitigating spurious forces and torques applied to the knee joint. Given the absence of a self-alignment mechanism, during the clinical investigation, special attention was paid to ensure proper initial alignment between the robot axis and the user's knee axis during the donning process. Nevertheless, we acknowledge that this initial alignment may not fully mitigate the issue of a mismatch between the human and robot joint axes.

The performance of the low-level controller of the AKO-β was considered suitable to assist common daily life activities of poststroke patients [37], [40], [42], with torque bandwidth

(>9 Hz) and parasitic torque (< 1.75 N·m up to 2.5 Hz) comparable with other SEA-based actuators [25], [26], [27].

B. AKO-β Control and Gait Phase Estimation

When assisting individuals with gait impairments, a key factor to achieve the desired effects on the user's kinematics relates to the adaptiveness of the torque-versus-phase assistive action. The AKO-β middle-level controller grounds on a continuous gait phase estimator and a phase-locked torque designer to finely tune subject-specific assistance.

Continuous gait phase estimation is advantageous compared with finite state machines based on discrete phases [55], as the torque profile can be modulated continuously and adjusted finely to fit the specific requirements of a user. Furthermore, it presents the advantage of a continuous adaptive gait phase variable that avoids sudden abrupt reset and nonlinear or nonmonotonic increment of the phase as for other methods [56], [57], [58]. In this work, the gait phase estimation was based on the method previously presented for a hip exoskeleton [33], [34], here adapted to use the knee joint angle, showing performance comparable with other state-of-the-art methods for continuous phase estimation [56], [57], [58]. In addition, the capability to measure the joint angle through the embedded joint encoder allows to maintain the exoskeleton self-contained and, thus, improve the overall usability of the device.

The gait phase estimator showed an *RMS phase reset error* lower than 2.5% of the gait cycle, which is lower than 4%, a value previously suggested by the literature as a threshold to have good synchrony between the biological torque and the assistance [34]. Such performance in terms of *RMS phase reset error* is comparable with previously published works, which report an error lower than 2.5% using sensorized insoles to measure the ground reaction forces [33], or lower than 2.05% when exploiting encoders to measure the two hip joint angles and detect heel-strike events [34]. To the best of the authors' knowledge, only one previous knee exoskeleton exploited an AOs-based controller, which was based on the hip angle of the unassisted leg measured by the thigh inertial measurement unit (IMU), achieving an estimated RMS error of 2.37% [19].

The good performance of the phase estimator shown in this work indicates that the method is robust even with knee angle profiles of impaired individuals. When used in AM, the performance is even more robust likely due to a more pronounced knee flexion peak due to the flexion assistance that makes the phase reset easier. Also, the gait phase estimator proved its robustness to slow gait speeds, which, for the three participants, ranged from 1 to 3 km/h. However, the decreased stride variability caused by treadmill walking poses a limitation for evaluating the controller's performance.

Deeper analyses must be performed to confirm these preliminary results during overground walking and with a greater number of poststroke participants showing different levels of impairment, particularly when knee flexion profiles are not pronounced, such as in the cases of a very stiff knee.

The segmentation of the gait phase based on the knee flexion peak represents a limitation of the current controller, as the timing of the peak flexion may vary across trials and conditions. Future work will focus on developing a heel-strike detection method based on angular kinematics, in line with approaches previously adopted in hip exoskeleton control [34].

Finally, the AKO-β controller will require a high-level layer for the automatic recognition of the user's locomotion and to adapt consequently the desired torque computed in the middle level. This high-level controller will be a part of future development, similar to previous studies on hip exoskeletons [59].

C. Pilot Experiments With Poststroke Participants

All three participants were assisted by the AKO-β with a flexion torque during the push-off and initial swing phase to enhance the reduced knee flexion of the participants consequent to stiff knee (ID1 and ID3) and muscle weakness (ID2). The tuned assistance significantly increased the knee flexion during the swing phase (+44.9% across participants) in the AM compared with the NoExo condition. Each participant had a similar increment (+26.85° for ID1, 18.05° for ID2, and +21.71° for ID3), despite the differences in the amplitude of the assistive torque delivered, consequent to the differences in body characteristics and impairments. Furthermore, the effects of the AKO-β assistance resulted in a clinically meaningful increment of the ROM of the paretic knee in the sagittal plane, of more than double the MCID of 8.48° in all three participants [53].

To the best of the authors' knowledge, only the SERKA exoskeleton was used to enhance the knee flexion of poststroke individuals, providing 30 N·m and resulting in a greater increment of the flexion angle compared with the results reported in this study [25]. However, the two participants assisted by the SERKA exhibited almost no voluntary knee flexion while walking. The increase of knee flexion observed here is particularly noteworthy when compared with other joint-targeted assistive devices in the state-of-the-art. Ankle–foot orthoses, although widely prescribed for poststroke individuals, have shown no effectiveness in improving knee kinematics during the swing phase [60]. Likewise, hip exoskeletons have shown minimal impact on knee gait kinematics under similar treadmill conditions [44]. Consistent with previous studies [61], [62], no differences in hip hiking were observed in AM compared with the NoExo conditions. However, hip abduction increased (7.48° across participants) in the AM condition compared with NoExo. This finding aligns with a previous study reporting increased hip abduction when knee flexion assistance is provided at foot-off, likely reflecting an altered motor pattern following the stroke rather than a purely compensatory strategy [61].

Here, by means of the middle-level controller of the AKO-β, the assistive flexion torque was also exploited to mitigate the hyperextension of ID1 and ID3. Hence, a decrement of their knee maximum extension angle (−3.64° for ID1 and −580° for ID3) was observed in AM compared with the NoExo condition. To date, no other knee exoskeleton has specifically targeted knee hyperextension in poststroke individuals. A comparable improvement of an across-participant increase of 9.7° in maximum knee extension was reported in a feasibility study using a quasi-direct-drive bilateral knee exoskeleton on young adults

with cerebral palsy. However, in contrast to the present findings, two of the five participants exhibited excessive midstance flexion, deviating from physiological kinematic patterns, as a result of the exoskeleton assistance [20].

The extension torque provided by the AKO-β was used with ID3 to compensate for the effects induced by the spasticity, achieving a smoother knee kinematic profile. Nevertheless, the greater variability of the knee kinematic profiles in the late swing phase and of the knee flexion peak (63.70° (49.00, 66.20)) in AM compared with the NoExo for ID3 suggests that the assistance may not have been effective consistently across all strides. This variability could have also been influenced by the participant walking while holding the handrails. However, these results suggest that AKO-β assistance may have the potential to mitigate spasticity in chronic poststroke individuals. Future studies should investigate further this application, additionally including the assessment of possible long-term effects in acute or subacute poststroke individuals within clinical settings.

The AKO-β extension torque could also support the users during the stance phase in cases of knee instability or buckling. Although ID2 reported knee buckling at enrollment, no instability episodes or notable kinematic deficits were observed during the sessions to warrant specific assistive tuning.

Overall, the immediate effect of the AKO-β assistance led to a more physiological knee kinematic profile on the paretic side, as indicated by the reduced GVS (-27.3% across participants) compared with the NoExo condition. However, a reassessment under more natural overground walking conditions would be required, considering the reduced stride variability promoted by the treadmill.

Although the AKO-β assistance was not targeting directly the hip joint, all three participants showed an increment of the hip flexion during the swing phase consequent to the additional external knee flexion moment generated by the exoskeleton ($+10.67°$ for ID1, 11.92° for ID2, and $+10.06°$ for ID3 in AM compared with NoExo). These hip and knee kinematics modifications may additionally contribute to having a greater paretic limb ground clearance [63]. No improvements were induced on the limited ankle plantarflexion, particularly visible in the kinematics' profiles of ID2 and ID3.

Temporal and spatial symmetry results indicated some slight improvements in two out of three participants, but the results were not conclusive and may need further investigation. Longer familiarization, in particular, may be necessary to enhance gait symmetry, thus improving hemiparetic gait pattern significantly [64]. In a similar study, the REFLEX exoskeleton led to improved symmetry index compared with the condition without exoskeleton in three hemiparetic participants, although the TM hampered the symmetry of two participants, which may limit the adoption of the assistive device [19].

The TM walking condition was assessed additionally with the participants to evaluate the capability of the AKO-β to reject disturbances due to the variability of the hemiparetic knee movement. Compared with the NoExo condition, the kinematics profiles in TM suggest that the AKO-β did not hinder the participants' gait, considering the additional weight on the user's leg and, concurrently, suggesting adequate "transparency" of the device. Nevertheless, the participants' kinematics in TM showed slight modifications compared with the NoExo condition, maybe due to placebo effects from wearing the device or to momentum effects from the actuator weight. Further investigation involving a larger cohort of participants is necessary to clarify these effects.

In this pilot study, none of the participants reported discomfort while using the AKO-β. While this study did not include the evaluation of the usability of the AKO-β, which was used with the constant supervision of engineers and therapists, future studies will be devoted to investigate the user's experience after appropriate training for autonomous and prolonged use.

The treadmill-based protocol included extended familiarization (at least 20 min) and provided the option to use handrails to ensure safety and build participants' confidence, given their frailty. Future studies should additionally consider overground walking to enable a more comprehensive assessment of balance, postural control, and changes in gait speed.

Participants showed different clinical conditions and motor impairments, allowing for a preliminary evaluation of the device's feasibility in clinical settings. Specifically, ID1 and ID3 exhibited stiff knee gait due to hyperactive quadriceps during the swing phase, while ID2 presented knee flexor weakness. Concerning gait impairments in the stance phase, ID1 and ID3 exhibited knee hyperextension due to abnormal hamstring activation, whereas ID2 experienced knee buckling.

This pilot study shows the feasibility of using AKO-β to mitigate gait impairments. However, further investigations are necessary to explore which conditions can be treated consistently. Future studies should include larger, gender-balanced chores and conduct deficit-specific analyses to achieve statistically significant results. To support broader inclusion, particularly of female participants, multiple sizes of the commercially available knee brace must be customized.

Acknowledgment

The authors would like to thank S. Doronzio, G. Arnetoli, A. Giffone, and R. Molino Lova for their support during the clinical investigation.

References

[1] GBD 2019 Stroke Collaborators, "Global, regional, and national burden of stroke and its risk factors, 1990–2019: A systematic analysis for the global burden of disease study 2019," *Lancet Neurol.*, vol. 20, no. 10, pp. 795–820, Oct. 2021, doi: 10.1016/S1474-4422(21)00252-0.

[2] D. J. Newham and S.-F. Hsiao, "Knee muscle isometric strength, voluntary activation and antagonist co-contraction in the first six months after stroke," *Disabil. Rehabil.*, vol. 23, no. 9, pp. 379–386, 2001, doi: 10.1080/0963828001006656.

[3] D. K. Sommerfeld, E. U.-B. Eek, A.-K. Svensson, L. W. Holmqvist, and M. H. von Arbin, "Spasticity after stroke: Its occurrence and association with motor impairments and activity limitations," *Stroke*, vol. 35, no. 1, pp. 134–139, Jan. 2004, doi: 10.1161/01.STR.0000105386.05173.5E.

[4] L. R. Sheffler and J. Chae, "Hemiparetic gait," *Phys. Med. Rehabil. Clin. North Amer.*, vol. 26, no. 4, pp. 611–623, Nov. 2015, doi: 10.1016/j.pmr.2015.06.006.

[5] E. Hong, "Comparison of quality of life according to community walking in stroke patients," *J. Phys. Ther. Sci.*, vol. 27, no. 7, pp. 2391–2393, 2015, doi: 10.1589/jpts.27.2391.

[6] J. Lexell, U.-B. Flansbjer, A. M. Holmbäck, D. Downham, and C. Patten, "Reliability of gait performance tests in men and woman with hemiparesis after stroke," *J. Rehabil. Med.*, vol. 37, no. 2, pp. 75–82, Mar. 2005, doi: 10.1080/16501970410017215.

[7] S. M. Woolley, "Characteristics of gait in hemiplegia," *Topics Stroke Rehabil.*, vol. 7, no. 4, pp. 1–18, 2001, doi: 10.1310/JB16-V04F-JAL5-H1UV.

[8] B. Balaban and F. Tok, "Gait disturbances in patients with stroke," *PM&R, J. Injury, Function, Rehabil.*, vol. 6, no. 7, pp. 635–645, 2014, doi: 10.1016/j.pmrj.2013.12.017.

[9] B. Zacharias and A. Kannenberg, "Clinical benefits of stance control orthosis systems: An analysis of the scientific literature," *JPO J. Prosthetics Orthotics*, vol. 24, no. 1, pp. 2–7, 2012.

[10] A. Zissimopoulos, S. Fatone, and S. A. Gard, "Biomechanical and energetic effects of a stance-control orthotic knee joint," *J. Rehabil. Res. Develop.*, vol. 44, no. 4, pp. 503–513, 2007, doi: 10.1682/JRRD.2006.09.0124.

[11] R. J. Ratcliffe and K. G. Holt, "Low frequency shock absorption in human walking," *Gait Posture*, vol. 5, no. 2, pp. 93–100, Apr. 1997, doi: 10.1016/S0966-6362(96)01077-6.

[12] E. Pröbsting, A. Kannenberg, and B. Zacharias, "Safety and walking ability of KAFO users with the C-brace orthotronic mobility system, a new microprocessor stance and swing control orthosis," *Prosthetics Orthotics Int.*, vol. 41, no. 1, pp. 65–77, Feb. 2017, doi: 10.1177/0309364616637954.

[13] T. Yan, M. Cempini, C. M. Oddo, and N. Vitiello, "Review of assistive strategies in powered lower-limb orthoses and exoskeletons," *Robot. Auton. Syst.*, vol. 64, pp. 120–136, Feb. 2015, doi: 10.1016/j.robot.2014.09.032.

[14] P. Beyl, M. Van Damme, R. Van Ham, B. Vanderborght, and D. Lefeber, "Pleated pneumatic artificial muscle-based actuator system as a torque source for compliant lower limb exoskeletons," *IEEE/ASME Trans. Mechatron.*, vol. 19, no. 3, pp. 1046–1056, Jun. 2014, doi: 10.1109/TMECH.2013.2268942.

[15] A. J. Veale, K. Staman, and H. Van Der Kooij, "Soft, wearable, and pleated pneumatic interference actuator provides knee extension torque for sit-to-stand," *Soft Robot.*, vol. 8, no. 1, pp. 28–43, Feb. 2021, doi: 10.1089/soro.2019.0076.

[16] M. Cestari, D. Sanz-Merodio, J. C. Arevalo, and E. Garcia, "An adjustable compliant joint for lower-limb exoskeletons," *IEEE/ASME Trans. Mechatron.*, vol. 20, no. 2, pp. 889–898, Apr. 2015, doi: 10.1109/TMECH.2014.2324036.

[17] T. Bacek, M. Moltedo, C. Rodriguez-Guerrero, J. Geeroms, B. Vanderborght, and D. Lefeber, "Design and evaluation of a torque-controllable knee joint actuator with adjustable series compliance and parallel elasticity," *Mech. Mach. Theory*, vol. 130, pp. 71–85, Dec. 2018, doi: 10.1016/j.mechmachtheory.2018.08.014.

[18] Y. Zhu, Q. Wu, B. Chen, D. Xu, and Z. Shao, "Design and evaluation of a novel torque-controllable variable stiffness actuator with reconfigurability," *IEEE/ASME Trans. Mechatron.*, vol. 27, no. 1, pp. 292–303, Feb. 2022, doi: 10.1109/TMECH.2021.3063374.

[19] J. S. Lora-Millan, F. J. Sanchez-Cuesta, J. P. Romero, J. C. Moreno, and E. Rocon, "A unilateral robotic knee exoskeleton to assess the role of natural gait assistance in hemiparetic patients," *J. NeuroEng. Rehabil.*, vol. 19, no. 1, Oct. 2022, Art. no. 109, doi: 10.1186/s12984-022-01088-2.

[20] D. Lee et al., "Reducing knee hyperextension with an exoskeleton in children and adolescents with genu recurvatum: A feasibility study," *IEEE Trans. Biomed. Eng.*, vol. 70, no. 12, pp. 3312–3320, Dec. 2023, doi: 10.1109/TBME.2023.3282165.

[21] C. K. Wong, L. Bishop, and J. Stein, "A wearable robotic knee orthosis for gait training: A case-series of hemiparetic stroke survivors," *Prosthetics Orthotics Int.*, vol. 36, no. 1, pp. 113–120, Mar. 2012, doi: 10.1177/0309364611428235.

[22] C. B. Sanz-Morère et al., "An active knee orthosis with a variable transmission ratio through a motorized dual clutch," *Mechatronics*, vol. 94, Oct. 2023, Art. no. 103018, doi: 10.1016/j.mechatronics.2023.103018.

[23] C. Nesler, G. Thomas, N. Divekar, E. J. Rouse, and R. D. Gregg, "Enhancing voluntary motion with modular, backdrivable, powered hip and knee orthoses," *IEEE Robot. Automat. Lett.*, vol. 7, no. 3, pp. 6155–6162, Jul. 2022, doi: 10.1109/LRA.2022.3145580.

[24] Z. Wu, M. Yang, Y. Xia, and L. Wang, "Mechanical structural design and actuation technologies of powered knee exoskeletons: A review," *Appl. Sci.*, vol. 13, no. 2, Jan. 2023, Art. no. 1064, doi: 10.3390/app13021064.

[25] J. S. Sulzer, R. A. Roiz, M. A. Peshkin, and J. L. Patton, "A highly backdrivable, lightweight knee actuator for investigating gait in stroke," *IEEE Trans. Robot.*, vol. 25, no. 3, pp. 539–548, Jun. 2009, doi: 10.1109/TRO.2009.2019788.

[26] S. V. Sarkisian, M. K. Ishmael, G. R. Hunt, and T. Lenzi, "Design, development, and validation of a self-aligning mechanism for high-torque powered knee exoskeletons," *IEEE Trans. Med. Robot. Bionics*, vol. 2, no. 2, pp. 248–259, May 2020, doi: 10.1109/TMRB.2020.2981951.

[27] M. K. Shepherd and E. J. Rouse, "Design and validation of a torque-controllable knee exoskeleton for sit-to-stand assistance," *IEEE/ASME Trans. Mechatron.*, vol. 22, no. 4, pp. 1695–1704, Aug. 2017, doi: 10.1109/TMECH.2017.2704521.

[28] K. Kong, J. Bae, and M. Tomizuka, "A compact rotary series elastic actuator for human assistive systems," *IEEE/ASME Trans. Mechatron.*, vol. 17, no. 2, pp. 288–297, Apr. 2012, doi: 10.1109/TMECH.2010.2100046.

[29] B. Celebi, M. Yalcin, and V. Patoglu, "AssistOn-knee: A self-aligning knee exoskeleton," in *Proc. IEEE/RSJ Int. Conf. Intell. Robots Syst.*, Tokyo, Japan, 2013, pp. 996–1002, doi: 10.1109/IROS.2013.6696472.

[30] M. del C. Sanchez-Villamañan, J. Gonzalez-Vargas, D. Torricelli, J. C. Moreno, and J. L. Pons, "Compliant lower limb exoskeletons: A comprehensive review on mechanical design principles," *J. NeuroEng. Rehabil.*, vol. 16, no. 1, Dec. 2019, Art. no. 55, doi: 10.1186/s12984-019-0517-9.

[31] M. Tiboni, A. Borboni, F. Vérité, C. Bregoli, and C. Amici, "Sensors and actuation technologies in exoskeletons: A review," *Sensors*, vol. 22, no. 3, Jan. 2022, Art. no. 884, doi: 10.3390/s22030884.

[32] S. Campagnini, P. Liuzzi, A. Mannini, R. Riener, and M. C. Carrozza, "Effects of control strategies on gait in robot-assisted post-stroke lower limb rehabilitation: A systematic review," *J. NeuroEng. Rehabil.*, vol. 19, no. 1, Dec. 2022, Art. no. 52, doi: 10.1186/s12984-022-01031-5.

[33] T. Yan, A. Parri, V. Ruiz Garate, M. Cempini, R. Ronsse, and N. Vitiello, "An oscillator-based smooth real-time estimate of gait phase for wearable robotics," *Auton. Robots*, vol. 41, no. 3, pp. 759–774, Mar. 2017, doi: 10.1007/s10514-016-9566-0.

[34] C. Livolsi, R. Conti, F. Giovacchini, N. Vitiello, and S. Crea, "A novel wavelet-based gait segmentation method for a portable hip exoskeleton," *IEEE Trans. Robot.*, vol. 38, no. 3, pp. 1503–1517, Jun. 2022, doi: 10.1109/TRO.2021.3122975.

[35] J. de Miguel-Fernández, J. Lobo-Prat, E. Prinsen, J. M. Font-Llagunes, and L. Marchal-Crespo, "Control strategies used in lower limb exoskeletons for gait rehabilitation after brain injury: A systematic review and analysis of clinical effectiveness," *J. NeuroEng. Rehabil.*, vol. 20, no. 1, Feb. 2023, Art. no. 23, doi: 10.1186/s12984-023-01144-5.

[36] C. Lee, S. Kwak, J. Kwak, and S. Oh, "Generalization of series elastic actuator configurations and dynamic behavior comparison," *Actuators*, vol. 6, 2017, Art. no. 26, doi: 10.3390/act6030026.

[37] G. Bovi, M. Rabuffetti, P. Mazzoleni, and M. Ferrarin, "A multiple-task gait analysis approach: Kinematic, kinetic and EMG reference data for healthy young and adult subjects," *Gait Posture*, vol. 33, no. 1, pp. 6–13, Jan. 2011, doi: 10.1016/j.gaitpost.2010.08.009.

[38] E. Reznick, K. R. Embry, R. Neuman, E. Bolívar-Nieto, N. P. Fey, and R. D. Gregg, "Lower-limb kinematics and kinetics during continuously varying human locomotion," *Sci. Data*, vol. 8, no. 1, Oct. 2021, Art. no. 282, doi: 10.1038/s41597-021-01057-9.

[39] S. J. Olney, M. P. Griffin, and I. D. McBride, "Temporal, kinematic, and kinetic variables related to gait speed in subjects with hemiplegia: A regression approach," *Phys. Ther.*, vol. 74, no. 9, pp. 872–885, Sep. 1994, doi: 10.1093/ptj/74.9.872.

[40] H. Ridgway, E. Bisson, and B. Brouwer, "A review of the physical demands of stair negotiation in healthy aging and following stroke," *Phys. Med. Rehabil. Int.*, vol. 2, 2015, Art. no. 1057.

[41] A. C. Novak and B. Brouwer, "Strength and aerobic requirements during stair ambulation in persons with chronic stroke and healthy adults," *Arch. Phys. Med. Rehabil.*, vol. 93, no. 4, pp. 683–689, Apr. 2012, doi: 10.1016/j.apmr.2011.10.009.

[42] G. Roy, S. Nadeau, D. Gravel, F. Piotte, F. Malouin, and B. J. McFadyen, "Side difference in the hip and knee joint moments during sit-to-stand and stand-to-sit tasks in individuals with hemiparesis," *Clin. Biomech.*, vol. 22, no. 7, pp. 795–804, Aug. 2007, doi: 10.1016/j.clinbiomech.2007.03.007.

[43] R. C. Browning, J. R. Modica, R. Kram, and A. Goswami, "The effects of adding mass to the legs on the energetics and biomechanics of walking," *Med. Sci. Sports Exercise*, vol. 39, pp. 515–525, 2007.

[44] C. Livolsi et al., "Bilateral hip exoskeleton assistance enables faster walking in individuals with chronic stroke-related gait impairments," *Sci. Rep.*, vol. 15, no. 1, Jan. 2025, Art. no. 2017, doi: 10.1038/s41598-025-86343-x.

[45] A. Baldoni, M. Fantozzi, and N. Vitiello, "A planar torsional spring," WO2020104962A1, May 2020. [Online]. Available: https://patents.google.com/patent/US20220003292A1/en

[46] K. Shamaei, G. S. Sawicki, and A. M. Dollar, "Estimation of quasi-stiffness of the human knee in the stance phase of walking," *PLoS One*, vol. 8, no. 3, Mar. 2013, Art. no. e59993, doi: 10.1371/journal.pone.0059993.

[47] R. B. Davis, S. Ounpuu, D. Tyburski, and J. R. Gage, "A gait analysis data collection and reduction technique," *Hum. Movement Sci.*, vol. 10, pp. 575–587, 1991, doi: 10.1016/0167-9457(91)90046-Z.

[48] A. Rodríguez-Fernández et al., "Comparing walking with knee-ankle-foot orthoses and a knee-powered exoskeleton after spinal cord injury: A randomized, crossover clinical trial," *Sci. Rep.*, vol. 12, no. 1, Nov. 2022, Art. no. 19150, doi: 10.1038/s41598-022-23556-4.

[49] S. Galle, P. Malcolm, W. Derave, and D. De Clercq, "Adaptation to walking with an exoskeleton that assists ankle extension," *Gait Posture*, vol. 38, no. 3, pp. 495–499, Jul. 2013, doi: 10.1016/j.gaitpost.2013.01.029.

[50] J. A. Zeni, J. G. Richards, and J. S. Higginson, "Two simple methods for determining gait events during treadmill and overground walking using kinematic data," *Gait Posture*, vol. 27, no. 4, pp. 710–714, May 2008, doi: 10.1016/j.gaitpost.2007.07.007.

[51] R. Baker et al., "The gait profile score and movement analysis profile," *Gait Posture*, vol. 30, no. 3, pp. 265–269, Oct. 2009, doi: 10.1016/j.gaitpost.2009.05.020.

[52] S. Nadeau, "Understanding spatial and temporal gait asymmetries in individuals post stroke," *Int. J. Phys. Med. Rehabil.*, vol. 2, no. 3, 2014, Art. no. 201, doi: 10.4172/2329-9096.1000201.

[53] A. Guzik, M. Drużbicki, A. Wolan-Nieroda, A. Turolla, and P. Kiper, "Estimating minimal clinically important differences for knee range of motion after stroke," *J. Clin. Med.*, vol. 9, no. 10, Oct. 2020, Art. no. 3305, doi: 10.3390/jcm9103305.

[54] Y. Lee et al., "Flexible gait enhancing mechatronics system for lower limb assistance (GEMS L-type)," *IEEE/ASME Trans. Mechatron.*, vol. 24, no. 4, pp. 1520–1531, Aug. 2019, doi: 10.1109/TMECH.2019.2922977.

[55] R. Baud, A. R. Manzoori, A. Ijspeert, and M. Bouri, "Review of control strategies for lower-limb exoskeletons to assist gait," *J. NeuroEng. Rehabil.*, vol. 18, no. 1, Dec. 2021, Art. no. 119, doi: 10.1186/s12984-021-00906-3.

[56] H. Eken et al., "Continuous phase estimation in a variety of locomotion modes using adaptive dynamic movement primitives," in *Proc. Int. Conf. Rehabil. Robot.*, Singapore, 2023, pp. 1–6, doi: 10.1109/ICORR58425.2023.10304682.

[57] I. Kang, D. D. Molinaro, S. Duggal, Y. Chen, P. Kunapuli, and A. J. Young, "Real-time gait phase estimation for robotic hip exoskeleton control during multimodal locomotion," *IEEE Robot. Automat. Lett.*, vol. 6, no. 2, pp. 3491–3497, Apr. 2021, doi: 10.1109/LRA.2021.3062562.

[58] X. Chen et al., "A piecewise monotonic gait phase estimation model for controlling a powered transfemoral prosthesis in various locomotion modes," *IEEE Robot. Automat. Lett.*, vol. 7, no. 4, pp. 9549–9556, Oct. 2022, doi: 10.1109/LRA.2022.3191945.

[59] A. Pergolini et al., "Real-time locomotion recognition algorithm for an active pelvis orthosis to assist lower-limb amputees," *IEEE Robot. Automat. Lett.*, vol. 7, no. 3, pp. 7487–7494, Jul. 2022, doi: 10.1109/LRA.2022.3183936.

[60] S. Tyson, E. Sadeghi-Demneh, and C. Nester, "A systematic review and meta-analysis of the effect of an ankle-foot orthosis on gait biomechanics after stroke," *Clin. Rehabil.*, vol. 27, no. 10, pp. 879–891, Oct. 2013, doi: 10.1177/0269215513486497.

[61] J. S. Sulzer, K. E. Gordon, Y. Y. Dhaher, M. A. Peshkin, and J. L. Patton, "Preswing knee flexion assistance is coupled with hip abduction in people with stiff-knee gait after stroke," *Stroke*, vol. 41, no. 8, pp. 1709–1714, Aug. 2010, doi: 10.1161/STROKEAHA.110.586917.

[62] J. de Miguel Fernández et al., "Adapted assistance and resistance training with a knee exoskeleton after stroke," *IEEE Trans. Neural Syst. Rehabil. Eng.*, vol. 31, pp. 3265–3274, Aug. 2023, doi: 10.1109/TNSRE.2023.3303777.

[63] F. Matsuda et al., "Analysis of strategies used by hemiplegic stroke patients to achieve toe clearance," *Jpn. J. Comprehensive Rehabil. Sci.*, vol. 7, pp. 111–118, 2016, doi: 10.11336/jjcrs.7.111.

[64] K. K. Patterson, W. H. Gage, D. Brooks, S. E. Black, and W. E. McIlroy, "Evaluation of gait symmetry after stroke: A comparison of current methods and recommendations for standardization," *Gait Posture*, vol. 31, no. 2, pp. 241–246, Feb. 2010, doi: 10.1016/j.gaitpost.2009.10.014.